

Multichannel excitation of the Yu-Shiba-Rusinov states of a molecular spin

Carmen Rubio-Verdú,^{1,2} Javier Zaldívar,¹ Rok Žitko,^{3,4} and José Ignacio Pascual^{1,5}

¹*CIC nanoGUNE-BRTA, 20018 Donostia-San Sebastián, Spain*

²*Department of Physics, Columbia University, New York 10027, United States*

³*Jožef Stefan Institute, Jamova 39, SI-1000 Ljubljana, Slovenia*

⁴*Faculty of Mathematics and Physics, University of Ljubljana, Jadranska 19, SI-1000 Ljubljana, Slovenia*

⁵*Ikerbasque, Basque Foundation for Science, 48013 Bilbao, Spain*

(Dated: December 22, 2024)

A magnetic impurity on a superconductor induces Yu-Shiba-Rusinov (YSR) bound states, detected in tunneling spectroscopy as narrow in-gap excitations. Hunds coupling is the energy scale that determines the impurity's magnetic ground state. However, experimental evidence that links the YSR nature with such fundamental intra-atomic exchange remains elusive. We report multichannel YSR states in a many-body molecular spin. We found that a magnetic porphyrin on Pb(111) exhibits two distinct YSR orbital interaction channels with identical intramolecular distribution of their particle-hole asymmetry. Supported by numerical calculations, we show that the YSR asymmetry is caused by orbitals with opposite potential scattering, coupled into a robust, spin-hosting molecular state, which also governs its normal state properties. Our results depict a new scenario for the study of entangled spin systems on superconductors using molecular platforms.

A magnetic impurity placed on a superconductor creates a spin-dependent scattering potential that locally distorts the bath of Cooper pairs and creates Yu-Shiba-Rusinov (YSR) bound states [1–3]. Such states are probed as quasiparticle excitations by tunneling electrons or holes. YSR states appear in tunneling spectra as pairs of narrow peaks inside the superconducting gap, at symmetric energy positions with respect to zero bias [4, 5]. The exchange coupling J between impurity and superconductor determines the position of its excitation peaks inside the gap. However, the number, spectral shape and spatial distribution of YSR states also depend on the nature of the interacting entire system, both substrate and impurity, offering additional information to study the magnetic ground state of atomic and molecular systems. In this Letter, we study YSR states induced by a many body molecular spin on a superconducting surface.

Magnetic molecules on superconductors generally show one single YSR channel [6–13], indicating weak hybridization with the substrate, although this channel can appear split due to the effect of intrinsic molecular spin/vibration excitations [7, 8, 10, 14, 15], or by interactions with other magnetic species [9]. However, atomic and molecular species with high spin may exhibit multiple YSR channels, reflecting the manifold of spin-carrying orbitals. Such multichannel picture has been observed for some 3d transition metals [4, 16, 17], where the orbital shapes were identified in the spatial distribution of the corresponding YSR state. While these orbital channels fulfil the predictions by Rusinov [3], they behave as independent channels and the effect of their intra-impurity magnetic exchange was absent in the observations.

Here, we report the multichannel YSR configuration of a magnetic iron porphyrin on the superconductor Pb(111). The identical particle-hole asymmetry of both YSR channels along the molecular axis, and its reversal

over the molecular center, reveals the presence of two spin-carrying molecular states with opposite sign potential scattering amplitude. With the support of numerical models, we show that both states are linked through strong Hunds-like intramolecular exchange, thus behaving as a many-body molecular state with integer spin, interacting with the substrate via two YSR channels. By comparison of the YSR regime with the normal state, where a Kondo resonance is found, we determine that the molecular spin lays in a weak interaction regime.

Our experiments were performed in a Scanning Tunneling Microscope (STM) with a base temperature of 1.2 K under UHV conditions (JT-STM by SPECS GmbH). We deposited chlorinated Fe-tetraphenyl porphyrin (FeTPP) molecules on a clean Pb(111) substrate at room temperature, which lose their chlorine ion upon adsorption [21]. On some metallic surfaces [18, 22], FeTPP preserves its $S = 1$ spin state, albeit Fe(II) complexes can also adopt a higher integer spin state on metals [23–26]. The Pb(111) surface accommodates an incommensurate square molecular lattice of FeTPP forming a moiré superstructure [6, 7], visible in Fig. 1a as segments of brighter and darker molecules. The darker species show a rather low hybridization with the substrate and are characterized by inelastic spin excitations outside the superconducting gap [18, 27, 28]. The brighter molecules, however, show YSR in-gap states, indicative of a stronger hybridization with the Pb(111) substrate. Here we focus on the regime of interactions that govern such brighter molecules.

We performed high-resolution dI/dV spectroscopy using a superconducting lead-terminated tip to enhance the energy resolution beyond the thermal limit [6, 29–31] (Fig. 1c). In addition to the characteristic double coherence peaks of the Pb(111) surface at $V_S \approx \pm 2.7$ mV [32] (Δ_1 and Δ_2 in Fig. 1c), the spectra show two pairs

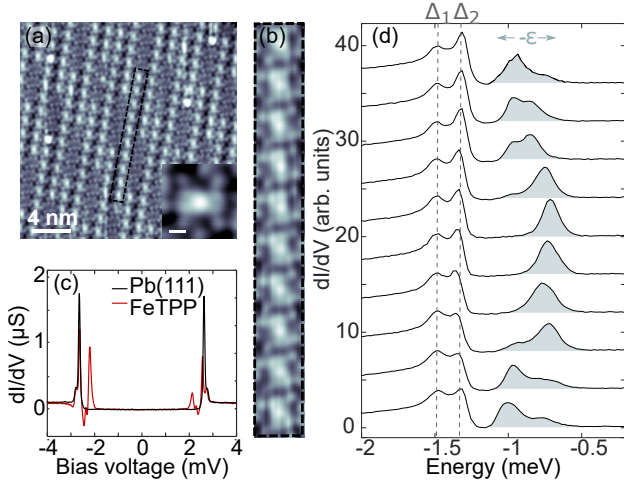


FIG. 1. (a) STM topography of a FeTPP molecular island showing the moiré pattern. (inset) STM topography of a single bright molecule. The two-fold shape is due to a saddle-shape conformation acquired by the porphine core, with two pairs of nonequivalent pyrroles [18]. The scale bar represents 4 Å. (b) STM topography of a bright molecular segment ($V_S = 45$ mV, $I = 100$ pA). (c) dI/dV spectrum on a FeTPP molecule obtained with a superconducting tip. The bare Pb(111) spectrum is shown in black as a reference ($V_S = 4$ mV, $I = 100$ pA). (d) dI/dV spectra of bright FeTPP molecules along the moiré line in b. The plots are obtained by numerically deconvolving the tip's superconducting density of states from dI/dV spectra, as described in [17]. Analysis of STM and STS data was performed with the WSxM [19] and SpectraFox [20] software packages.

of sub-gap peaks, that we attribute to the excitation of two YSR bound states [1–3, 5]. The YSR peaks appear at bias voltages spanning from ± 2.0 to ± 2.3 mV, depending on the molecule. By deconvolving the tip's superconducting gap from the spectra (Fig. 1d), we find that the YSR excitation energies lie in the range $0.5\Delta_1 \lesssim \epsilon_i \lesssim 0.7\Delta_1$. The two YSR peaks frequently follow the trend shown in Fig. 1d: their position, separation, and amplitude change from one molecule to another. The energy ϵ_i is lower in molecular sites around the center of the bright moiré segments, and lie closer to the coherence peaks at the ends. The variations of YSR peaks' position along the lines reflect an increasing overlap of the incommensurate molecular lattice with the lead surface atoms towards the center [6, 27]: the smaller ϵ_i values can be attributed to a larger magnetic exchange J between molecular spin and substrate Cooper pairs. This behaviour indicates that the two peaks correspond to two distinct YSR interaction channels, rather than a single channel split by intrinsic (spin or vibrational) molecular excitations [7, 14, 15, 33].

Both YSR channels display a characteristic asymmetry in the intensity of their particle (p) and hole (h) components. The p-h asymmetry is not homogeneous within the molecule, but exhibits an intramolecular spatial distribution (see Fig. 2). Spectra on pyrrole and Fe

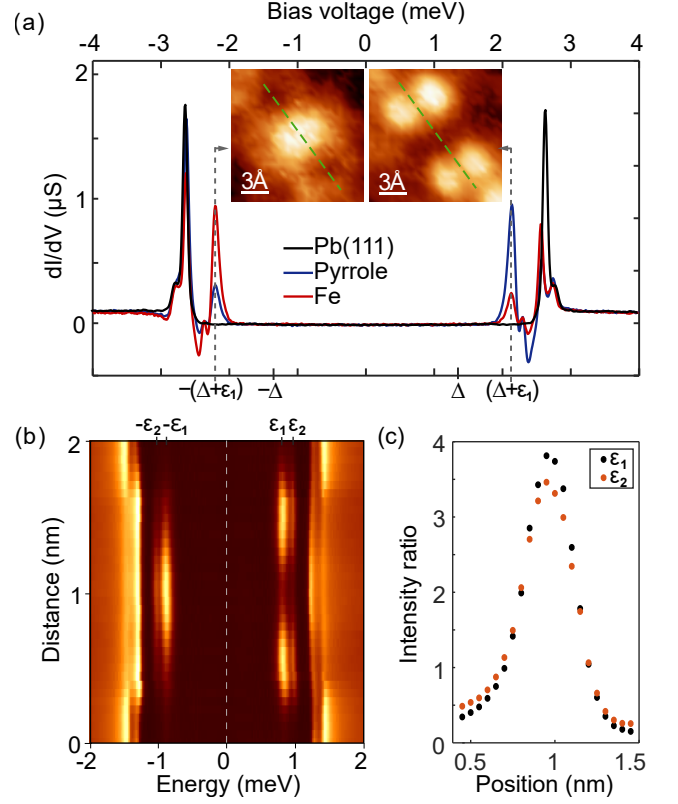


FIG. 2. (a) dI/dV spectroscopy on the pyrrole (blue) and iron (red) sites of a FeTPP molecule. Inset: Constant current dI/dV maps at the energy of the hole and electron components of the YSR states, respectively. (b) Stacking plot of point dI/dV along the FeTPP, numerically deconvolved using the method in ref. [17]. ($V_S = 4$ mV, $I = 100$ pA). (c) The ratio between peak's amplitudes at each polarity ($A_i(V > 0)/A_i(V < 0)$) follows the same trend for both YSR excitations.

sites show the same YSR peaks but the amplitude of their particle and hole components is reversed (see Fig. 2). Over the pyrrole groups (see Fig. 2a), the positive YSR peaks appear more intense, while over the Fe ion hole-like excitations ($V_S < 0$) are stronger. This intriguing p-h asymmetry pattern is identical for both ϵ_1 and ϵ_2 peaks (Figs. 2b,c), and is observed in all the bright molecules of the moiré. Such p-h asymmetry is usually interpreted in terms of the hybridization between the low-energy molecular levels and the superconductor, which breaks p-h symmetry in the normal state in the presence of a finite potential scattering amplitude \mathcal{U} [34, 35]. In terms of the single-impurity Anderson model, a negative (positive) potential scattering corresponds to a singly occupied energy level ϵ_d close (far) to E_F [i.e. $\epsilon_d < U_d/2$ ($\epsilon_d > U_d/2$), U_d is the Coulomb charging energy] leading to Bogoliubov quasiparticle (BQ) excitations in the superconducting state with larger hole (particle) components [36–41].

The asymmetry pattern is consistent with a multi-orbital molecular spin with two YSR interaction channels on the Pb(111) surface, where the variations of the YSR particle-hole asymmetry across the molecule are caused by the different distribution and energy alignment of the spin-hosting orbitals. However, the identical intensity pattern followed by both ϵ_1 and ϵ_2 YSR peaks indicates that they cannot be treated as two independent orbital channels, as in refs. [16, 17]. Instead, we consider here that intramolecular (Hund's-like) exchange is strong ($J_H \gg \Delta$) and the total molecular spin behaves as a robust many-body spin state composed of different orbitals strongly interacting, and coupled with the superconductor via two channels. In this scenario, both YSR channels can be indistinguishably excited by electrons tunneling through each of the two molecular orbitals. This case is the superconducting analog of the inelastic excitation pattern of the $S = 1$ molecular spin found for Fe(II) complexes on Au(111) [18, 25].

To validate such multichannel YSR picture in the presence of local variations of potential scattering, we simulated low-energy spectra using numerical renormalization group (NRG) calculations. We considered two singly-occupied orbitals with opposite potential scattering amplitudes and interacting via intramolecular exchange coupling to build up a molecular $S = 1$ state. The effective Hamiltonian takes the following form:

$$\begin{aligned}
 H_{\text{imp}} &= \sum_{n=1,2} \epsilon_{d,n} \sum_{\sigma} d_{n,\sigma}^{\dagger} d_{n,\sigma} + \sum_{n=1,2} U_{d,n} n_{n,\uparrow} n_{n,\downarrow} \\
 &\quad - J_H \mathbf{S}_1 \cdot \mathbf{S}_2 + g \mu_B B S_{z,\text{total}}, \\
 H_{\text{BCS}} &= \sum_{i,k\sigma} \epsilon_k c_{i,k\sigma}^{\dagger} c_{i,k\sigma} + \sum_{i,k} \Delta c_{i,k\uparrow}^{\dagger} c_{i,k\downarrow}^{\dagger} + \text{H.c.} \\
 H_{\text{hyb}} &= \sum_{n,i} \sum_{k\sigma} V_{n,i} d_{n,\sigma}^{\dagger} c_{i,k\sigma} + \text{H.c.}, \\
 H_{\text{tunnel}} &= \sum_{n,\sigma} t_n d_{n,\sigma}^{\dagger} c_{\text{tip},\sigma} + \text{H.c.},
 \end{aligned} \tag{1}$$

Here $n = 1, 2$ indexes the molecular orbitals and $i = 1, 2$ the combinations of substrate electron states that form the different screening channels; $d_{n,\sigma}$ and $c_{i,k\sigma}$ are the corresponding operators. The molecule is described by a two-orbital Anderson impurity model with on-site energies $\epsilon_{d,n}$ and electron-electron repulsion energies $U_{d,n}$, and an inter-orbital direct exchange (or Hund's) coupling J_H that aligns the spins ferromagnetically. The Zeeman term caused by an external magnetic field B is also included. The operators are $n_{n,\sigma} = d_{n,\sigma}^{\dagger} d_{n,\sigma}$, $\mathbf{S}_n = (1/2) \sum_{\alpha\beta} d_{n,\alpha}^{\dagger} \boldsymbol{\sigma}_{\alpha\beta} d_{n,\beta}$ and $S_{z,\text{total}} = S_{z,1} + S_{z,2}$. The substrate is described by two copies of the BCS Hamiltonian, one for each screening channel. The hybridization of molecular orbitals and substrate electrons is given by the matrix elements $V_{n,i}$, which are chosen to

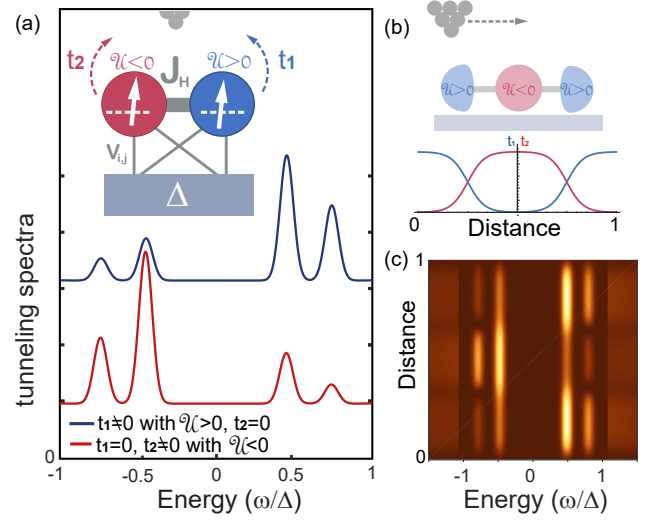


FIG. 3. (a) Simulated tunneling spectral functions for two orbitals with strong Hund's coupling $J_H = 0.3$ (in units of the (half)bandwidth) and with potential scattering \mathcal{U} of opposite sign (model parameters $U_{d,1} = U_{d,2} = 3$, $\epsilon_{d,1} = -0.25$ and $\epsilon_{d,2} = -2.74$, the density of states in the band is $\rho = 0.5$ and the BCS gap is $\Delta = 10^{-3}$). We plot results for the case of both orbitals weakly hybridized with the substrate with matrix elements $V_{1,1} = V_{2,1}$ and $V_{2,2} = -V_{1,2}$, such that $\pi\rho V_{1,1}^2 = 0.05$ and $\pi\rho V_{2,2}^2 = 0.035$. The orbitals are coupled with an STM tip via hopping constants t_1 and t_2 . (b) Simulated spatial dependence of the tunneling hopping used in (c) to account for the experimental distribution of p-h asymmetry. (c) Spectral map of YSR excitations with tunneling hopping in (b).

obtain YSR state energies in the experimental range.

To account for the spatial variations of \mathcal{U} in the spectral maps, we included a spatial-dependent coupling term with a STM tip through the term H_{tunnel} in eq. 1. We simulated two orbitals with potential scattering \mathcal{U} of opposite sign, as suggested by the experiments. The resulting tunneling spectra [Fig. 3(a)] reproduce the key experimental findings: the two channels are indistinguishably excited by electron tunneling through either orbital, and both YSR excitations show a clear p-h asymmetry dictated by the \mathcal{U} of the orbital selected by the STM tip. The spatial variations of p-h asymmetry are readily simulated by inserting a spatial dependence to the tunneling constants t_n [Fig. 3(b)]. The resulting spectral map modulates the YSR amplitudes according to the molecular orbital picked up by the STM tip at every site [Fig. 3(c)], thus reproducing the intramolecular p-h asymmetry observed in the experiments.

The multi-channel excitation and its response to \mathcal{U} is only obtained in the presence of strong Hund's coupling. We also note that the precise effect of the p-h asymmetry on \mathcal{U} depends on the regime of hybridization amplitude $V_{n,i}$: in the weak regime (free-like spin) the YSR p-h asymmetry reproduces that of the normal state DOS

(as in Fig. 3), but this behavior is reversed for channels in the strong-interacting regime (Kondo-screened) [7, 42]. According to this behavior, the identical p-h asymmetry pattern followed by both channels in the experiment is the result of both lying in the same interaction regime (i.e. we exclude an underscreened-like configuration formed by the combination of a strong channel and a weak one).

The interaction regime of each of the two channels can be interrogated in the normal-state. To quench superconductivity in both sample and tip, we applied an external magnetic field of $B = 0.5$ T. In Fig. 4a we compare the dI/dV features obtained over the Fe and pyrrole sites of the FeTPP molecule, where we find zero-bias features compatible with Kondo physics. On the pyrroles, a sharp zero-bias resonance appears in the low-energy spectra. On the center of the FeTPP molecule, the resonance has an asymmetric dip lineshape associated to a larger Fano-like interference over the Fe site.

The Kondo resonance exhibits an enhanced sensitivity to the external magnetic field. A sizable splitting is resolved at a magnetic field of $B^* \approx 2$ T (Fig. 4c). Tak-

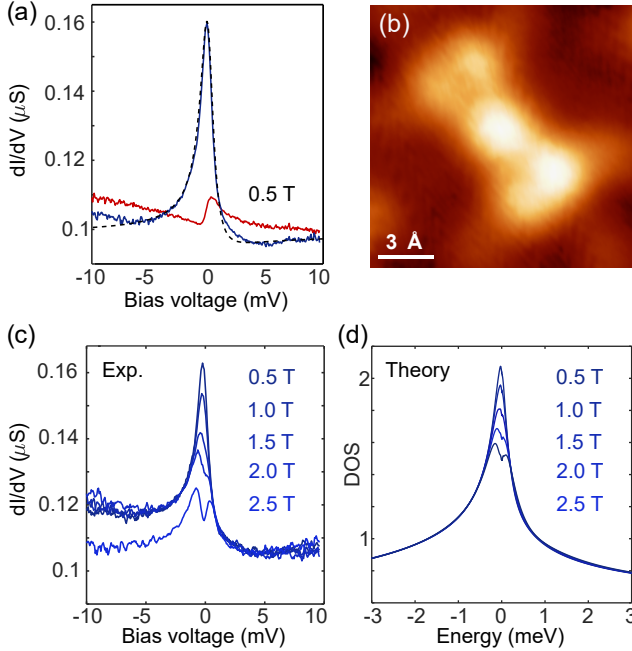


FIG. 4. (a) dI/dV spectroscopy of a bright FeTPP molecule once superconductivity has been quenched on both tip and sample at $B = 0.5$ T. ($V_S = 15$ mV, $I = 1$ nA). (b) Constant-height conductance map obtained at $V_S = 100$ μ V showing the spatial distribution of the Kondo resonance. The central round protrusion lies over the Fe site. Two-fold symmetric lobes over each bright pyrrole groups. (c) dI/dV spectra of FeTPP molecule as the out-of-plane magnetic field is increased ($V_S = 15$ mV, $I = 300$ pA). (d) Simulated spectra and splitting with magnetic field for the parameter set used in Fig. 3

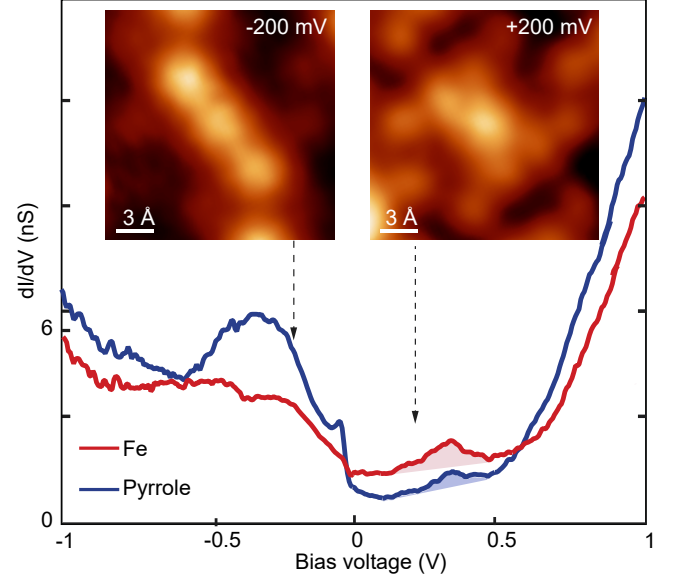


FIG. 5. Wide-range dI/dV spectra of a bright molecule ($V_S = 1.5$ V, $I = 3$ nA, $V_{rms} = 2$ mV). Inset: Constant height conductance maps measured at $V_S = -200$ mV and $V_S = +200$ mV, respectively ($I = 200$ pA).

ing into account the thermal broadening, such field is consistent with the weak-coupling regime with a Kondo temperature below the experimental temperature. We simulated the spectral function in the normal state using parametrization regimes that reproduce the positions of the experimental YSR peaks, comparing the regimes of weak and strong hybridization. For the later case, the Kondo linewidth is significantly larger than the experimental one and cannot be split by the applied magnetic field. For the weak hybridization scenario of Fig. 3, however, there is a narrow resonance due to a weak-Kondo interaction regime [8, 43] that splits with B , thus reproducing the experimental finding in the normal state (Fig. 4d).

The distribution of the Kondo resonance reveals the shape of the many-body orbital hosting the molecular spin [44–46]. A constant height spatial map of the Kondo amplitude (dI/dV at $V \sim 0$, Fig. 4b) reproduces an elongated shape composed of a round protrusion over the Fe site and two-fold symmetric lobes over the bright pyrrole groups. This image resembles the YSR amplitude maps in the superconducting state (inset in Fig. 2(a)), where particle and hole components are localized on pyrrole or Fe sites, respectively.

This extended molecular state can be related to a combination of frontier molecular states pictured in Fig. 5. A resonance at 400 meV above E_F appears extended over the pyrrole groups with a shape similar to that found in the Kondo and YSR maps. From its alignment and shape, we conclude that this corresponds to a spin-hosting molecular orbital with $\mathcal{U} > 0$, thus responsible

for larger YSR particle components over the molecular sides. Below E_F the spectra is dominated by a manifold of molecular states, with strong weight over the organic ligand and over the Fe ion. Here, the most probable scenario is that the Fe ion hosts a second spin-carrying state (as in ref. [18]) contributing to the total molecular spin. Given its alignment right below E_F , this state has opposite potential scattering ($\mathcal{U} < 0$) and leads to inverted particle-hole asymmetry over the center.

In summary, our results demonstrate the existence of a multichannel Yu-Shiba-Rusinov picture describing the interaction of the molecular spin of the Fe(II) complex FeTPP with superconducting Pb(111). The particle-hole asymmetry of both pairs of sub-gap Yu-Shiba-Rusinov excitations describes the same intramolecular distribution. With the support of NRG calculations we find that FeTPP molecules have a robust many-body spin interacting with the substrate through two weakly screening channels. In this multichannel configuration both YSR channels are excited similarly by electron tunneling through each molecular orbitals, while their particle-hole symmetry is governed by the tunneling pathway selected by the STM tip. The scenario depicted here provides evidences for novel quantum regimes for spins on superconductors, where intra-molecular Hund's exchange govern the magnetic behaviour even in a multichannel hybridization.

We thank Laetitia Farinacci, Felix von Oppen, and Katharina Franke for discussions and for sharing with us their work before submission. We gratefully acknowledge financial support from Spanish AEI and the European Regional Development Fund (ERDF) (MAT2016-78293-C6 and the Maria de Maeztu Units of Excellence Programme MDM-2016-0618), and from the European Union (EU) through Horizon 2020 (FET-Open project SPRING Grant. no. 863098). CRV acknowledges funding from the European Unions Horizon 2020 research and innovation programme under the Marie Skłodowska-Curie grant agreement No 844271. R. Ž. is supported by Slovenian Research Agency (ARRS) under Program P1-0044.

-
- [1] L. Yu, *Acta Physica Sinica* **21**, 75 (1965).
 - [2] H. Shiba, *Prog. Theor. Phys.* **40**, 435 (1968).
 - [3] A. I. Rusinov, *Sov. J. Exp. Theor. Phys.* **29**, 1101 (1969).
 - [4] S.-H. Ji, T. Zhang, Y.-S. Fu, X. Chen, X.-C. Ma, J. Li, W.-H. Duan, J.-F. Jia, and Q.-K. Xue, *Phys. Rev. Lett.* **100**, 226801 (2008).
 - [5] B. W. Heinrich, J. I. Pascual, and K. J. Franke, *Prog. Surf. Sci.* **93**, 1 (2018), [arXiv:1705.03672](#).
 - [6] K. J. Franke, G. Schulze, and J. I. Pascual, *Science* **332**, 940 (2011).
 - [7] N. Hatter, B. W. Heinrich, M. Ruby, J. I. Pascual, and K. J. Franke, *Nat. Commun.* **6**, 8988 (2015), [arXiv:1509.09108](#).
 - [8] N. Hatter, B. W. Heinrich, D. Rolf, and K. J. Franke, *Nat. Commun.* **8**, 2016 (2017), [arXiv:1710.04599](#).
 - [9] S. Kezilebieke, M. Dvorak, T. Ojanen, and P. Liljeroth, *Nano Lett.* **18**, 2311 (2018), [arXiv:1701.03288](#).
 - [10] S. Kezilebieke, R. Žitko, M. Dvorak, T. Ojanen, and P. Liljeroth, *Nano Lett.* **19**, 4614 (2019), [arXiv:1811.11591](#).
 - [11] J. Brand, S. Gozdzik, N. Néel, J. L. Lado, J. Fernández-Rossier, and J. Kröger, *Phys. Rev. B* **97**, 195429 (2018).
 - [12] L. Malavolti, M. Briganti, M. Hänze, G. Serrano, I. Cimatti, G. McMurtrie, E. Otero, P. Ohresser, F. Totti, M. Mannini, R. Sessoli, and S. Loth, *Nano Lett.* **18**, 7955 (2018).
 - [13] M. Etzkorn, M. Eltschka, B. Jäck, C. R. Ast, and K. Kern, (2018), [arXiv:1807.00646](#).
 - [14] R. Žitko, O. Bodensiek, and T. Pruschke, *Phys. Rev. B - Condens. Matter Mater. Phys.* **83**, 30 (2011).
 - [15] D. Golež, J. Bonča, and R. Žitko, *Phys. Rev. B* **86**, 1 (2012).
 - [16] M. Ruby, Y. Peng, F. von Oppen, B. W. Heinrich, and K. J. Franke, *Phys. Rev. Lett.* **117**, 186801 (2016).
 - [17] D.-J. Choi, C. Rubio-Verdú, J. de Bruijckere, M. M. Ugeda, N. Lorente, and J. I. Pascual, *Nat. Commun.* **8**, 15175 (2017).
 - [18] C. Rubio-Verdú, A. Sarasola, D.-J. Choi, Z. Majzik, R. Ebeling, M. R. Calvo, M. M. Ugeda, A. Garcia-Lekue, D. Sánchez-Portal, and J. I. Pascual, *Commun. Phys.* **1**, 15 (2018), [arXiv:1708.01268](#).
 - [19] I. Horcas, R. Fernández, J. M. Gómez-Rodríguez, J. Colchero, J. Gómez-Herrero, and A. M. Baro, *Rev. Sci. Instr.* **78**, 013705 (2007).
 - [20] M. Ruby, *SoftwareX*. **5**, 31 (2016).
 - [21] B. W. Heinrich, G. Ahmadi, V. L. Miller, L. Braun, J. Pascual, and K. J. Franke, *Nano Lett.* **13**, 4840 (2013).
 - [22] S. Karan, C. García, M. Karolak, D. Jacob, N. Lorente, and R. Berndt, *Nano Lett.* **18**, 88 (2018).
 - [23] W. Wang, R. Pang, G. Kuang, X. Shi, X. Shang, P. N. Liu, and N. Lin, *Phys. Rev. B* **91**, 045440 (2015).
 - [24] B. Liu, H. Fu, J. Guan, B. Shao, S. Meng, J. Guo, and W. Wang, *ACS Nano* **11**, 11402 (2017).
 - [25] D. Rolf, C. Lotze, C. Czekelius, B. W. Heinrich, and K. J. Franke, *J. Phys. Chem. Lett.* **9**, 6563 (2018), [arXiv:1811.00059](#).
 - [26] D. Rolf, F. Maaß, C. Lotze, C. Czekelius, B. W. Heinrich, P. Tegeder, and K. J. Franke, *J. Phys. Chem. C* **123**, 7425 (2019).
 - [27] B. W. Heinrich, L. Braun, J. I. Pascual, and K. J. Franke, *Nat. Phys.* **9**, 765 (2013).
 - [28] B. W. Heinrich, L. Braun, J. I. Pascual, and K. J. Franke, *Nano Letters* **15**, 4024 (2015).
 - [29] S. H. Pan, E. W. Hudson, and J. C. Davis, *Appl. Phys. Lett.* **73**, 2992 (1998).
 - [30] H. Suderow, M. Crespo, P. Martinez-Samper, J. G. Rodrigo, G. Rubio-Bollinger, S. Vieira, N. Luchier, J. P. Brison, and P. C. Canfield, in *Phys. C Supercond. its Appl.*, Vol. 369 (North-Holland, 2002) pp. 106–112.
 - [31] J. G. Rodrigo, H. Suderow, and S. Vieira, *Eur. Phys. J. B* **40**, 483 (2004).
 - [32] M. Ruby, B. W. Heinrich, J. I. Pascual, and K. J. Franke, *Phys. Rev. Lett.* **114**, 157001 (2015), [arXiv:1409.6638](#).
 - [33] S. Pradhan and J. Fransson, (2020), [arXiv:2001.11725](#).
 - [34] J. R. Schrieffer and P. A. Wolff, *Phys. Rev.* **149**, 491 (1966).
 - [35] M. Ternes, *New Journal of Physics* **17**, 63016 (2015),

- [arXiv:1505.04430](#).
- [36] P. G. de Gennes, *Superconductivity of Metals and Alloys* (Addison-Wesley, New York, 1989).
 - [37] a. Balatsky, I. Vekhter, and J.-X. Zhu, *Rev. Mod. Phys.* **78**, 373 (2006).
 - [38] M. E. Flatté and J. M. Byers, *Phys. Rev. Lett.* **78**, 3761 (1997).
 - [39] M. I. Salkola, a. V. Balatsky, and J. R. Schrieffer, *Phys. Rev. B* **55**, 12648 (1997).
 - [40] Y. Kim, J. Zhang, E. Rossi, and R. M. Lutchyn, *Phys. Rev. Lett.* **114**, 236804 (2015), [arXiv:1410.4558v3](#).
 - [41] J. Bauer, J. I. Pascual, and K. J. Franke, *Phys. Rev. B* **87**, 075125 (2013), [arXiv:1208.3211](#).
 - [42] L. Farinacci, G. Ahmadi, G. Reecht, M. Ruby, N. Bogdanoff, O. Peters, B. W. Heinrich, F. Von Oppen, and K. J. Franke, *Phys. Rev. Lett.* **121**, 196803 (2018), [arXiv:1807.01344](#).
 - [43] Y. H. Zhang, S. Kahle, T. Herden, C. Stroh, M. Mayor, U. Schlickum, M. Ternes, P. Wahl, and K. Kern, *Nat. Commun.* **4**, 2110 (2013).
 - [44] J. Li, S. Sanz, M. Corso, D. J. Choi, D. Peña, T. Frederiksen, and J. I. Pascual, *Nat. Commun.* **10**, 200 (2019), [arXiv:1808.07532](#).
 - [45] M. Moro-Lagares, R. Korytár, M. Piantek, R. Robles, N. Lorente, J. I. Pascual, M. R. Ibarra, and D. Serrate, *Nat. Commun.* **10**, 2211 (2019).
 - [46] J. Li, S. Sanz, J. Castro-Esteban, M. Vilas-Varela, N. Friedrich, T. Frederiksen, D. Peña, and J. I. Pascual, *Phys. Rev. Lett.* **124**, 177201 (2020), [arXiv:1912.08298](#).